SUPPORTING INFORMATION - Synthesis and characterization of lignin hydrogels for potential applications as drug eluting antimicrobial coatings for medical materials.

Eneko Larrañeta, Mikel Imízcoz*, Jie X. Toh*, Nicola J. Irwin*, Anastasia Ripolin*, Anastasia Perminova*, Juan Domínguez-Robles**, Alejandro Rodríguez**, Ryan F. Donnelly*.*

* Queen's University, Belfast School of Pharmacy, 97 Lisburn Road, Belfast, BT9 7BL, United Kingdom.

** Universidad de Córdoba, Chemical Engineering Department Campus of Rabanales, building Marie Curie, Córdoba, 14071, Spain.

Total number of pages: 14

Total number of figures: 8

Total number of tables: 3

Corresponding author

Email: e.larraneta@qub.ac.uk

Tel: +44 (0)28 9097 2360

1. Lingnin characterization

The chemical composition of the used lignin is presented in Table S1. The dealkaline lignin was used as received, so it was initially unwashed. This sample showed a value of total lignin content around 80%, which is commonly considered the sum of Klason lignin (KL) and acid soluble lignin (ASL). The value of ASL was remarkably high, which is probably due to the severe cooking conditions of the employed pulping process, which would increase the proportion of low-molecular-weight lignin[1,2]. The number of inorganic particles (14.72%) is consistent with the results obtained by other researchers using the same type of lignin[3,4]. Part of these inorganics is the sulphur content found in the elemental analysis (2.34%) (Table S2). Also, the analytical techniques of ICP-OES and SEM-EDAX revealed the presence of Na and S[3,5]. All this, therefore, indicates that the used lignin might have been isolated performing a kaft process, since in this pulping method Na_2S and NaOH are used in different proportions as reagents[5]. The carbon and hydrogen contents (Table S2) are in the range of other technical lignins. In lignin samples, it is assumed that the Nitrogen content comes from cell proteins. The lignin used in this work, showed a Nitrogen (Table S2) content similar to wood lignin samples, which is much lower than those obtained from wheat straw lignin[6]. Finally, the absence of glucose in the carbohydrates analysed confirms that the cellulose is devoid of cellulose contamination (Table S1).

Table S1. Chemical composition of the LIG sample

Sample Component	Composition (%)
Total lignin	77.83 ± 0.83
Klason lignin	59.56 ± 0.94
Acid – soluble lignin	18.27 ± 0.03
Ash	14.72 ± 0.23
Total hemicellulose	ND
Glucose	ND
Xylose	ND
Arabinose	ND

Table S2. Elemental composition of the LIG sample

Element	Composition (%)
C	52.76
H	4.76
N	0.20
S	2.34

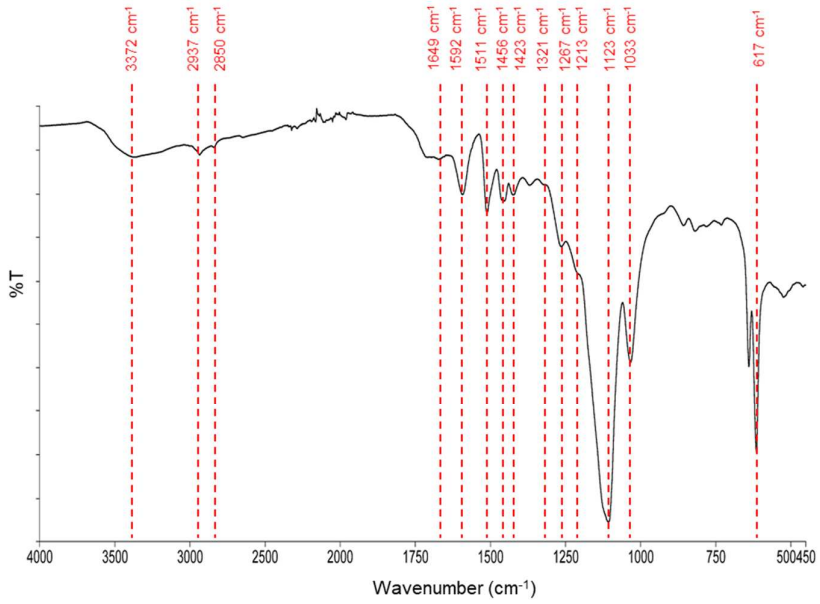

Figure S1. FTIR spectra of the LIG sample

The chemical structure of the employed lignin was studied using FTIR and Solid State ^{13}C-NMR. The FTIR of the lignin was recorded (Figure S1) and compared with the assignments found in other scientific papers[6-8]. As observed form the Figure S1, the dealkaline lignin shows a wide band centred at 3372 cm^{-1} corresponding to the aromatic and aliphatic OH groups. Moreover, bands located 2937 and 2850 cm^{-1} are assigned to the symmetrical and asymmetrical C-H stretching of the methyl and methylene groups, respectively. A band representing the asymmetric deformation of C-H stretching also appears at 1456 cm^{-1}. Additionally, the absorption bands located at 1592, 1511, and 1423 cm^{-1} were assigned to aromatic ring vibrations of the phenylpropane units. The observance of a band at 1649 cm^{-1} is due to stretching vibrations of conjugated carbonyl groups. The band at 1321 cm^{-1} can be assigned to C-O stretching in the syringyl units, which is typical for non-wood lignins[2]. Although the supplier does not give so much information about the pulping process or the raw material used, this band was practically inexistent in the used lignin sample which could indicate that a wood species was employed. Furthermore, bands located at 1267 and 1213 cm^{-1} are associated to guaiacyl units, indicating G ring and C=O stretch. Also, the intense band located at 1033 cm^{-1} could be assigned to stretching vibrations of C-H bonds in the guaiacyl structure. This band is less intense or even inexistent when the sample has a lower amount of G units[6]. The most intense band observed at 1123 cm^{-1} is assigned to C-O stretching in ether and alcohol groups. Finally, the band at 617 cm^{-1} was attributed to C-S stretching[7]. It also indicates that the lignin was isolated using a pulping process containing sulphur delignifying agents and/or was precipitated employing sulphuric acid.

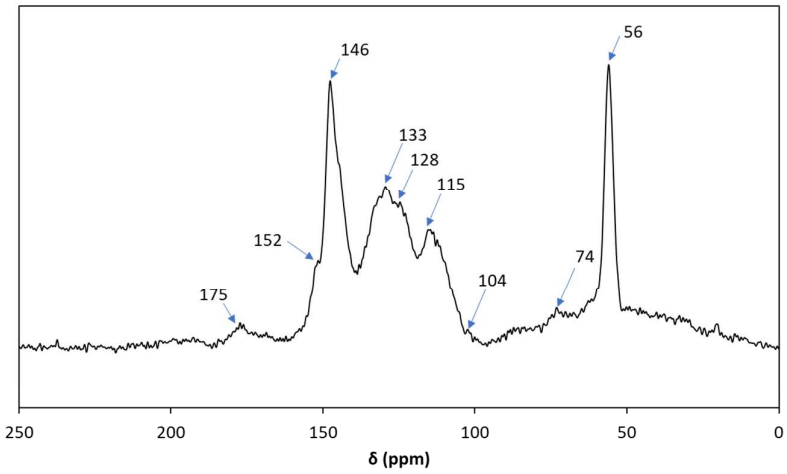

Figure S2. ^{13}C-CPMAS solid-state NMR spectrum of LIG.

The ^{13}C-Cross Polarization Magic Angle (CPMAS) solid-state NMR spectrum of the dealkaline lignin is shown in the Figure S2. The peak around 56 ppm has been attributed to the methoxyl groups[9]. According to the supplier this lignin has 11.1% of these groups (calcd. on anh. substance). The peaks around 74 and 104 ppm could be attributed to the resonance of carbons in carbohydrates moieties[2] and these two peaks are practically inexistent in the used lignin. This support the results found in the Table S1, where the analysed monomers are below the quantification limit. Lignin fracions with a high amount of carbohydrates (11-12% o.d.m.) showed marked peaks at 74 and 104 ppm[2]. Moreover, the peaks around 115 and 128 were ascribed to the C5 in Guaicayl units and to both C2 and C6 in *p*-hydroxyphenyl units, whereas the signal around 133 ppm was due to the C1 in Guaicayl and Syringil units[10]. Other peaks arising from the resonance of lignin carbons are those around 146 and 152 ppm, which were assigned to the resonance of C3/C5 in etherified Syringil units and of C3/C4 non-etherified Guaiacyl units, respectively[11]. Finally, the peaks between 165 and 185 have been attributed to carboxyl and ester groups of lignin[2].

2. FTIR analysis of the LIG-based hydrogels

Figure S3A shows the spectra of the pure components and of LIG10K before (LIG10K NC) and after the crosslinking process. The main difference is the formation of anhydride groups between the contiguous COOH groups in GAN[12,13]. However, these new anhydride groups are labile and disappear when the hydrogels are hydrated or over prolonged periods of time due to ambient humidity. A

further point of interest concerns the shift in the carbonyl peak (1760-1680 cm^{-1}) observed for the non-crosslinked materials when compared with pure GAN (Figure S3B). In pure GAN, there are non-covalent interactions, mainly hydrogen bonds, between the acid groups[14,15]. When GAN, LIG and PEG were combined, these interactions disappeared because GAN chains were mixed with the other molecules producing a shift in the peak to higher wavenumbers. The films containing GLY instead of PEG displayed a lower peak displacement. This suggests that the presence of GLY did not preclude the establishment of non-covalent interactions between GAN chains. This can be easily explained by the smaller size of the GLY molecule than the PEG molecules used in the present work.

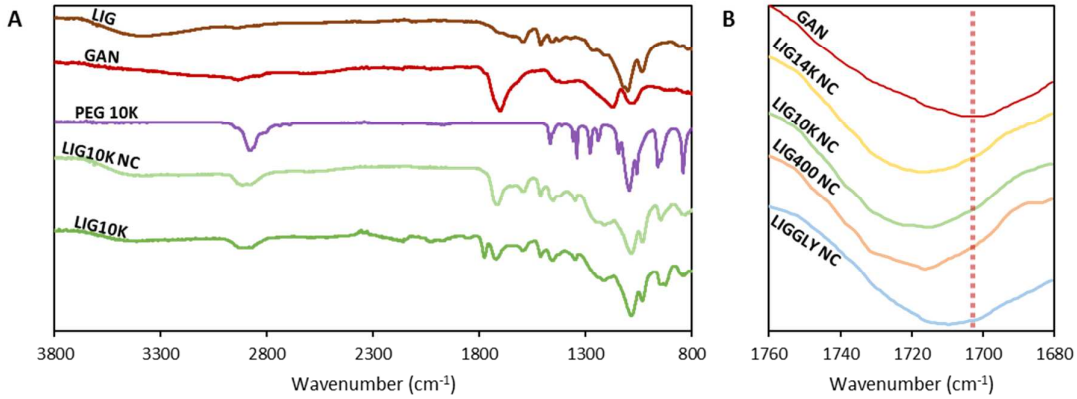

Figure S3. FTIR spectra of LIG, GAN, PEG 10K, non crosslinked LIG10K (LIG10K NC) and LIG10K (A). Carbonyl region of GAN and non-crosslinked LIG/GAN/PEG mixtures (B).

3. Solid state ^{13}C-NMR analysis of the LIG-based hydrogels

Figure S4A shows the solid state ^{13}C-NMR spectra for the major pure components of the hydrogels. It can be seen that some of the main peaks are not overlapping and, consequently, they have been used to estimate the sample composition. The peaks between 158 and 100 ppm were used for estimation of the concentration of LIG in the hydrogels. These signals are due to aromatic carbons in LIG and they are a unique identifier for LIG (Figure S4A)[16]. The peak between 185 and 165 ppm was used to estimate the concentration of GAN in the hydrogels. This peak can be assigned to the acid group carbons of GAN (see Figure S4A)[17]. Finally, the peak between 77 and 66 ppm was used to estimate the concentration of PEG in the hydrogels.

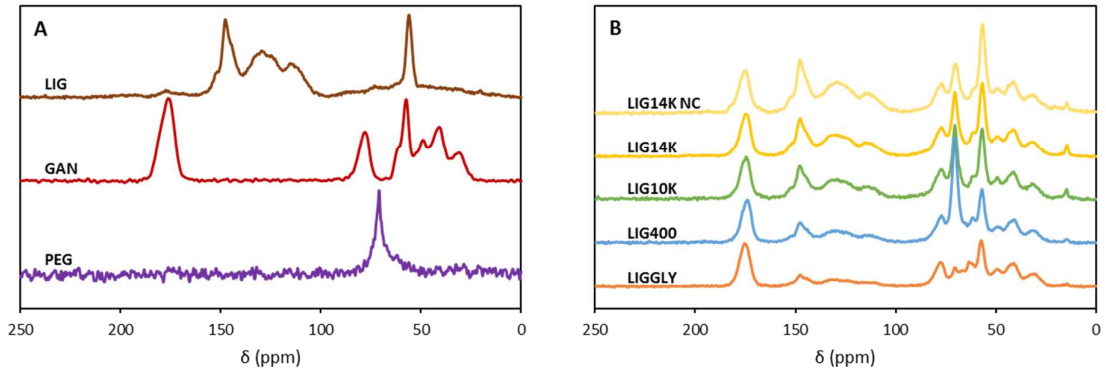

Figure S4. Solid state ^{13}C NMR spectra of LIG, GAN and PEG (A) and the hydrogels (B).

Figure S4B shows the solid state ^{13}C-NMR spectra of the LIG14K initial mixture (LIG14K NC) and of the other hydrogels after crosslinking and washing. In order to estimate the component percentages, the previously described peaks were used. The peak area ratio of LIG/GAN (area of the 158-100 ppm peak/area of the 185-165 ppm peak) and LIG/PEG (area of the 158-100 ppm peak/area of the 77-66 ppm peak) was calculated for the LIG14K NC sample and was used as a standard since the LIG:GAN:PEG ratio in LIG14K NC was known (2:1:1). The LIG/GAN and LIG/PEG peak area ratios were calculated for all synthesised hydrogels and compared with the standard. The obtained results are shown in Table 1 in the manuscript. The composition of the LIGGLY hydrogel could not be estimated due to the low intensity and overlap of the peak assigned to GLY at 77-66 ppm with peaks from GAN and LIG.

4. SEM Images of the LIG-based hydrogels

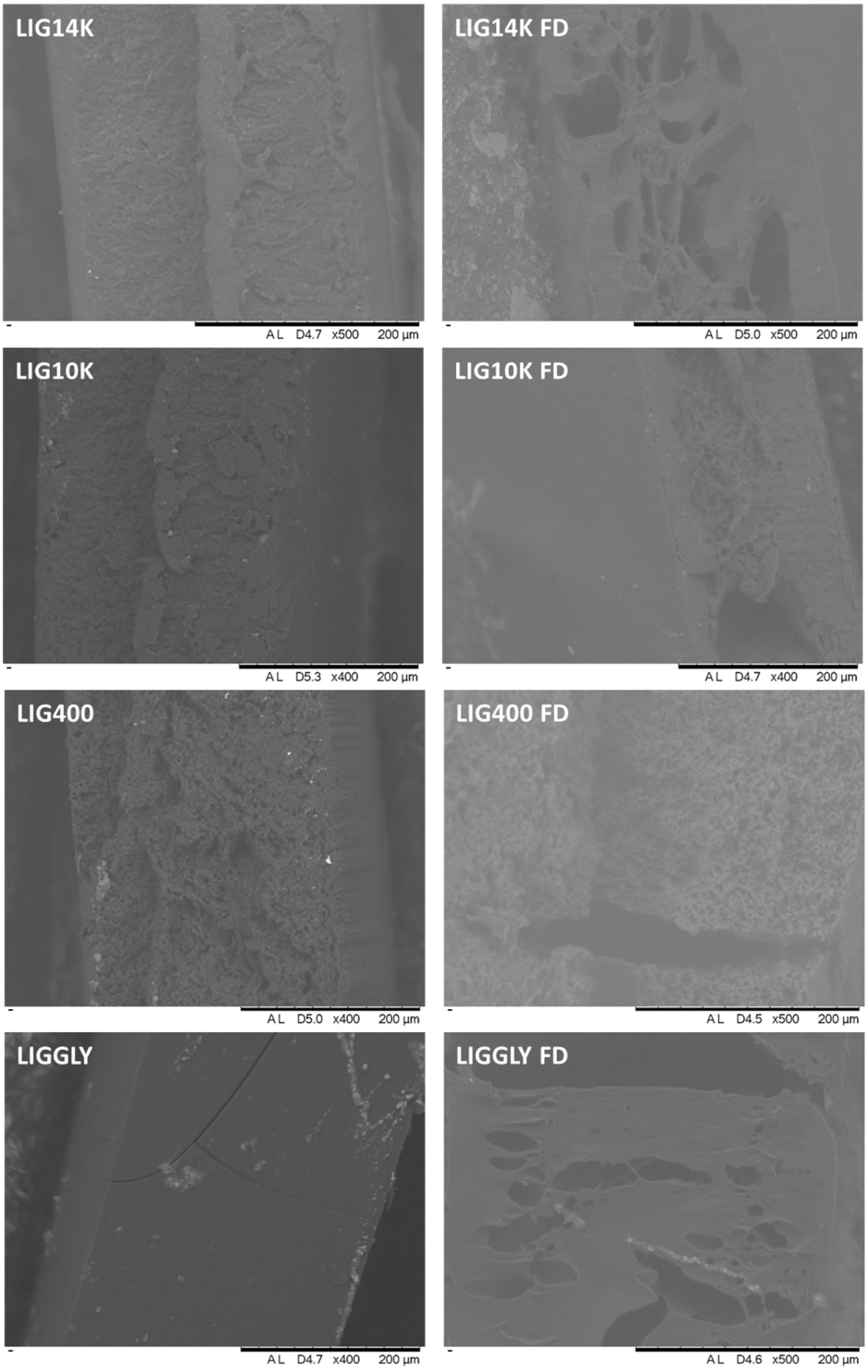

Figure S5. SEM images of the dry and freeze dried (FD) LIG-based hydrogels.

5. Curcumin release and mathematical modelling

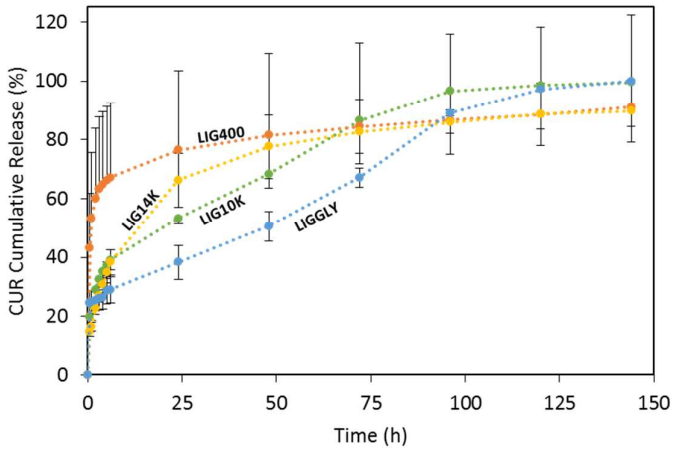

Figure S6. CUR cumulative release from all the LIG-containing hydrogels hydrogels (n=3).

Figure S6 shows the cumulative CUR release from the LIG-based hydrogels. Additionally, Table S3 shows the results obtained after fitting CUR relase data to different kinetic models. After fitting the release data (Figure S6) to the Korsmeyer-Peppas model, LIG14K showed an n value close to 0.45, indicating that Fickian diffusion was the main mechanism governing the release process[18,19]. This is consistent with the high correlation obtained after using the Higuchi model (Fickian diffusion model) for the release data from LIG14K hydrogels. In contrast, the other hydrogels showed lower n values suggesting a burst release. The CUR was rapidly released and did not follow a defined release mechanism. Consequently, these hydrogels displayed poor correlation with the Higuchi model as CUR release from these hydrogels did not follow a Fickian diffusion model. These models were applied to the sections of the release curves up to 60% of the CUR release. However, LIGGLY and LIG10K showed linear release after the initial burst release. Consequently, a Zero-Order model was applied to the linear segments of the curves for these two hydrogels. The results obtained after using a Zero-Order model for the linear range can be seen in Table 4. Both hydrogels showed similar k_{zo} indicating similar release kinetics. The only factor that can explain this behaviour is the similarities in the swelling profiles between these two hydrogels. However, LIG10K showed a superior release capability as these hydrogels were able to take up higher amounts of CUR.

Table S3. Results of fitting the release of CUR from different hydrogels to Korsmeyer-Peppas, Higuchi and Zero-Order models.

Hydrogel	Korsmeyer-Peppas			Higuchi		Zero-Order		
	k_{KP} (h^{-n})	n	R^2	k_H ($h^{-1/2}$)	R^2	Range (h)	k_{ZO} (h^{-1}) · 10^3	R^2
LIG14K	0.17 ± 0.01	0.43 ± 0.02	0.994	0.16 ± 0.01	0.987	-	-	-
LIG10K	0.25 ± 0.01	0.25 ± 0.01	0.998	0.14 ± 0.01	0.604	6.0-96.0	6.5 ± 0.3	0.991
LIG400	0.52 ± 0.01	0.23 ± 0.02	0.999	0.48 ± 0.01	0.919	-	-	-
LIGGLY	0.22 ± 0.01	0.19 ± 0.02	0.949	0.09 ± 0.01	0.156	0.5-96.0	6.4 ± 0.3	0.991

6. *In vitro* microbiological assessment

As shown in Figure S7, samples of GANPEG and LIG10K hydrogels demonstrated significantly greater resistance to adherence of both pathogens relative to PVC controls after challenge periods up to 24 h. Moreover, surfaces of unwashed LIG10K remained free of bacterial contamination during the initial 4 h incubation period and logarithmic reductions in adherence of *S. aureus* of up to 5.0 were achieved on surfaces of the 24 h-soaked lignin-containing materials relative to PVC controls during this same period. Importantly, the samples demonstrated no loss in antibacterial efficacy after soaking in deionised water for periods up to seven days. The surfaces of the materials remained free of contamination from both *S. aureus* and *P. mirabilis* during the initial 4 h challenge periods and relative percentage reductions of 99.8%, 99.6% and 99.6% in adherence of *S. aureus* were reported on unwashed, 24 h and seven-day pre-soaked samples, respectively, after 24 h incubation. Corresponding reductions after a 24 h challenge period with *P. mirabilis* were 97.2%, 97.8% and 92.6%, respectively, relative to PVC controls. The observed durability and retention of antibacterial properties after rinsing is important with regards to clinical application of the lignin-containing materials as medical device coating technologies, and the associated need for prevention of infection throughout the period of device implantation[20].

The resistance to bacterial adherence of the GAN- and PEG-crosslinked LIG hydrogels observed herein is expected to be a combined effect of the GAN, PEG and LIG components. Indeed, GAN AN 169 BF in the form of biodegradable microneedles has previously demonstrated antibacterial activity towards a range of Gram-positive and –negative pathogens, including *S. aureus* and *Escherichia coli*[21]. In addition, the inclusion of GAN S-97 within triclosan solutions has been reported to exert a synergistic effect on corresponding bactericidal activity towards endodontic pathogens including *Enterococcus faecalis*[22]. The antibacterial activity of PEG is also well established. For example, PEG 1000 has been reported to exhibit more potent bactericidal activity against *Streptococcus mutans* and *E. coli* than comparator vehicles such as propylene glycol and glycerine[23]. The significant

antibacterial activity of solutions of PEG 400 against various pathogens, including *Pseudomonas aeruginosa* and *Klebsiella pneumonia,* has been attributed to mechanisms involving reductions in the water activity, with resulting plasmolysis of cells, and direct interactions with bacterial cells, leading to clumping and changes in cell morphology[24]. Furthermore, chemical grafting of PEG onto thermoplastic polyurethane electrospun nanofibres with carbon nanotubes (CNT) not only reduced thecytotoxicity of CNT but also increased bacterial resistance of the prepared nanofibres[25].

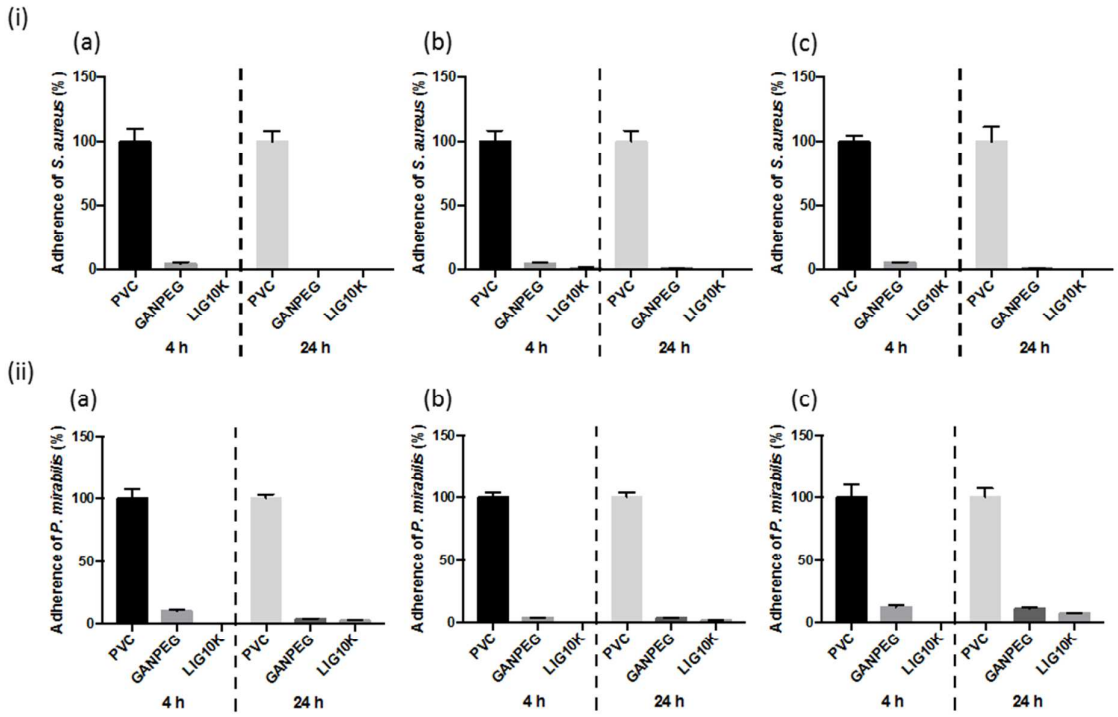

Figure S7. Adherence (%) of (i) *S. aureus* and (ii) *P. mirabilis* to surfaces of GANPEG and LIG10K pre-soaked in deionised water for (a) 0 h, (b) 24 h and (c) seven days relative to PVC controls after 4 h and 24 h incubation at 37°C. Columns and error bars represent means ± standard deviations ($n \geq 5$).

In Figure S8, the significantly higher resistance of the LIG10K samples pre-soaked for periods of 0 h, 24 h and seven days to adherence of *S. aureus* and *P. mirabilis* after 4 h and 24 h incubation relative to GANPEG controls can be seen. While this is the first report of the antibacterial properties of GAN- and PEG-crosslinked LIG hydrogels, LIG has previously demonstrated promising antimicrobial activities towards cultures of Gram-positive bacteria, including *Listeria monocytogenes* and *S. aureus,* and yeast, including *Candida lipolytica* [26,27]. The antimicrobial properties of lignin have previously been attributed to the polyphenolic components of this compound, which are reported to damage microbial cell membrane integrity with resultant bacterial lysis[28,29]. With respect to the

activity of LIG towards Gram-negative bacteria, mixed findings have been reported. No efficacy of LIG samples towards Gram-negative bacteria, including *Escherichia coli* and *Salmonella enterica,* and fungi, including *Aspergillus niger,* was reported in studies by Nada *et al.* and Dong *et al.* , whereas Yang *et al.* have recently demonstrated promising capacity of LIG-nanoparticle-containing nanocomposite films based on polyvinyl alcohol and chitosan in inhibiting the growth of two Gram-negative pathogens, *Pectobacterium carotovora* and *Xanthomonas arboricola*[26,30,31].

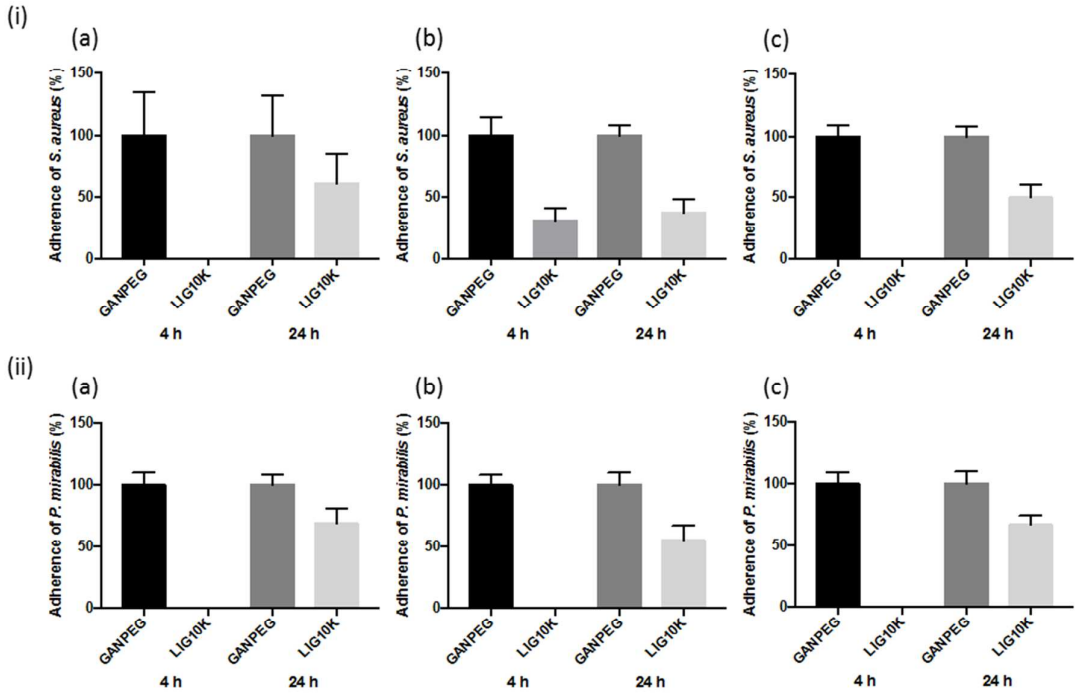

Figure S8. Adherence (%) of (i) *S. aureus* and (ii) *P. mirabilis* to surfaces of LIG10K pre-soaked in deionised water for (a) 0 h, (b) 24 h and (c) seven days relative to GANPEG controls after 4 h and 24 h incubation at 37°C. Columns and error bars represent means ± standard deviations ($n \geq 5$).

7. References

1. Domínguez-Robles, J.; Sánchez, R.; Díaz-Carrasco, P.; Espinosa, E.; García-Domínguez, M. T.; Rodríguez, A. Isolation and characterization of lignins from wheat straw: Application as binder in lithium batteries. *Int. J. Biol. Macromol.* **2017***, 104*, 909-918, DOI 10.1016/j.ijbiomac.2017.07.015.

2. Domínguez-Robles, J.; Sánchez, R.; Espinosa, E.; Savy, D.; Mazzei, P.; Piccolo, A.; Rodríguez, A. Isolation and Characterization of *Gramineae* and *Fabaceae* Soda Lignins. *Int. J. Mol. Sci.* **2017***, 18*, 327, DOI 10.3390/ijms18020327.

3. Deepa, A. K.; Dhepe, P. L. Solid acid catalyzed depolymerization of lignin into value added aromatic monomers. *RSC Adv.* **2014***, 4*, 12625-12629, DOI 10.1039/C3RA47818A.

4. Nandiwale, K. Y.; Danby, A. M.; Ramanathan, A.; Chaudhari, R. V.; Subramaniam, B. Zirconium-Incorporated Mesoporous Silicates Show Remarkable Lignin Depolymerization Activity. *ACS Sustainable Chem. Eng.* **2017***, 5*, 7155-7164, DOI 10.1021/acssuschemeng.7b01344.

5. Deepa, A. K.; Dhepe, P. L. Lignin Depolymerization into Aromatic Monomers over Solid Acid Catalysts. *ACS Catal.* **2015***, 5*, 365-379, DOI 10.1021/cs501371q.

6. Domínguez-Robles, J.; Tamminen, T.; Liitiä, T.; Peresin, M. S.; Rodríguez, A.; Jääskeläinen, A. S. Aqueous acetone fractionation of kraft, organosolv and soda lignins. *Int. J. Biol. Macromol.* **2018***, 106*, 979-987, DOI 10.1016/j.ijbiomac.2017.08.102.

7. Domínguez-Robles, J.; Espinosa, E.; Savy, D.; Rosal, A.; Rodríguez, A. Biorefinery Process Combining Specel® Process and Selective Lignin Precipitation using Mineral Acids. *Bioresources* **2016***, 11*, 7061-7077, DOI 10.15376/biores.11.3.7061-7077.

8. You, T. T.; Mao, J. Z.; Yuan, T. Q.; Wen, J. L.; Xu, F. Structural elucidation of the lignins from stems and foliage of Arundo donax Linn. *J. Agric. Food Chem.* **2013***, 61*, 5361-70, DOI 10.1021/jf401277v.

9. Savy, D.; Piccolo, A. Physical–chemical characteristics of lignins separated from biomasses for second-generation ethanol. *Biomass Bioenerg.* **2014***, 62*, 58-67, DOI 10.1016/j.biombioe.2014.01.016.

10. Nadji, H.; Diouf, P. N.; Benaboura, A.; Bedard, Y.; Riedl, B.; Stevanovic, T. Comparative study of lignins isolated from Alfa grass (Stipa tenacissima L.). *Bioresour. Technol.* **2009***, 100*, 3585-3592, DOI 10.1016/j.biortech.2009.01.074.

11. Savy, D.; Cozzolino, V.; Vinci, G.; Nebbioso, A.; Piccolo, A. Water-Soluble Lignins from Different Bioenergy Crops Stimulate the Early Development of Maize (Zea mays, L.). *Molecules* **2015***, 20*, 19958-19970, DOI 10.3390/molecules201119671.

12. Sclavons, M.; Franquinet, P.; Carlier, V.; Verfaillie, G.; Fallais, I.; Legras, R.; Laurent, M.; Thyrion, F. C. Quantification of the maleic anhydride grafted onto polypropylene by chemical and viscosimetric titrations, and FTIR spectroscopy. *Polymer* **2000***, 41*, 1989-1999, DOI 10.1016/S0032-3861(99)00377-8.

13. Larrañeta, E.; Lutton, R. E. M.; Brady, A. J.; Vicente-Pérez, E. M.; Woolfson, A. D.; Thakur, R. R. S.; Donnelly, R. F. Microwave-Assisted Preparation of Hydrogel-Forming Microneedle Arrays for Transdermal Drug Delivery Applications. *Macromol. Mater. Eng.* **2015***, 300*, 586-595, DOI 10.1002/mame.201500016.

14. Moolman, F. S.; Meunier, M.; Labuschagne, P. W.; Truter, P. A. Compatibility of polyvinyl alcohol and poly(methyl vinyl ether-co-maleic acid) blends estimated by molecular dynamics. *Polymer* **2005***, 46*, 6192-6200, DOI 10.1016/j.polymer.2005.03.121.

15. Larrañeta, E.; Henry, M.; Irwin, N. J.; Trotter, J.; Perminova, A. A.; Donnelly, R. F. Synthesis and characterization of hyaluronic acid hydrogels crosslinked using a solvent-free process for

potential biomedical applications. *Carbohydr. Polym.* **2018***, 181*, 1194-1205, DOI 10.1016/j.carbpol.2017.12.015.

16. Fu, L.; McCallum, S. A.; Miao, J.; Hart, C.; Tudryn, G. J.; Zhang, F.; Linhardt, R. J. Rapid and accurate determination of the lignin content of lignocellulosic biomass by solid-state NMR. *Fuel* **2015***, 141*, 39-45, DOI 10.1016/j.fuel.2014.10.039.

17. Calo, E.; Barros, J. M. S. d.; Fernandez-Gutierrez, M.; San Roman, J.; Ballamy, L.; Khutoryanskiy, V. V. Antimicrobial hydrogels based on autoclaved poly(vinyl alcohol) and poly(methyl vinyl ether-alt-maleic anhydride) mixtures for wound care applications. *RSC Adv.* **2016***, 6*, 55211-55219, DOI 10.1039/C6RA08234C.

18. Ritger, P. L.; Peppas, N. A simple equation for description of solute release I. Fickian and Non-Fickian release from non-swellable devices in the form of slabs, spheres, cylinders or discs. *J. Controlled Release* **1987***, 5*, 23-36, DOI 10.1016/0168-3659(87)90034-4.

19. Larrañeta E; Martínez-Ohárriz C; Vélaz I; Zornoza A; Machín R; Isasi JR In Vitro release from reverse poloxamine/α-cyclodextrin matrices: modelling and comparison of dissolution profiles. *J. Pharm. Sci.* **2014***, 103*, 197-206, DOI 10.1002/jps.23774.

20. Cheng, H.; Li, Y.; Huo, K.; Gao, B.; Xiong, W. Long-lasting in vivo and in vitro antibacterial ability of nanostructured titania coating incorporated with silver nanoparticles. *Journal of Biomedical Materials Research Part A* **2014***, 102*, 3488-3499, DOI 10.1002/jbm.a.35019.

21. Boehm, R. D.; Miller, P. R.; Singh, R.; Shah, A.; Stafslien, S.; Daniels, J.; Narayan, R. J. Indirect rapid prototyping of antibacterial acid anhydride copolymer microneedles. *Biofabrication* **2012***, 4*, 011002, DOI 10.1088/1758-5082/4/1/011002.

22. Nudera, W. J.; Fayad, M. I.; Johnson, B. R.; Zhu, M.; Wenckus, C. S.; BeGole, E. A.; Wu, C. D. Antimicrobial Effect of Triclosan and Triclosan with Gantrez on Five Common Endodontic Pathogens. *J Endod.* **2007***, 33*, 1239-1242, DOI 10.1016/j.joen.2007.06.009.

23. Nalawade, T. M.; Bhat, K.; Sogi, S. H. P. Bactericidal activity of propylene glycol, glycerine, polyethylene glycol 400, and polyethylene glycol 1000 against selected microorganisms. *J. Int. Soc. Prev. Community Dent.* **2015***, 5*, 114-119, DOI 10.4103/2231-0762.155736.

24. Chirife, J.; Herszage, L.; Joseph, A.; Bozzini, J. P.; Leardini, N.; Kohn, E. S. In vitro antibacterial activity of concentrated polyethylene glycol 400 solutions. *Antimicrob. Agents Chemother.* **1983***, 24*, 409-412.

25. Shi, H.; Liu, H.; Luan, S.; Shi, D.; Yan, S.; Liu, C.; Li, R. K. Y.; Yin, J. Effect of polyethylene glycol on the antibacterial properties of polyurethane/carbon nanotube electrospun nanofibers. *RSC Adv.* **2016***, 6*, 19238-19244, DOI 10.1039/C6RA00363J.

26. Dong, X.; Dong, M.; Lu, Y.; Turley, A.; Jin, T.; Wu, C. Antimicrobial and antioxidant activities of lignin from residue of corn stover to ethanol production. *Ind. Crops Prod.* **2011***, 34*, 1629-1634, DOI 10.1016/j.indcrop.2011.06.002.

27. Gabov, K.; Oja, T.; Deguchi, T.; Fallarero, A.; Fardim, P. Preparation, characterization and antimicrobial application of hybrid cellulose-lignin beads. *Cellulose* **2017***, 24*, 641-658, DOI 10.1007/s10570-016-1172-y.

28. Zemek, J.; Košíková, B.; Augustín, J.; Joniak, D. Antibiotic properties of lignin components. *Folia Microbiol.* **1979***, 24*, 483-486, DOI 10.1007/BF02927180.

29. Espinoza-Acosta, J., Torres-Chávez, P., Ramírez-Wong, B., López-Saiz, C., Montaño-Leyva,B. Antioxidant, Antimicrobial, and Antimutagenic Properties of Technical Lignins and Their Applications. *Bioresources* **2016***, 11*.

30. Yang, W.; Owczarek, J. S.; Fortunati, E.; Kozanecki, M.; Mazzaglia, A.; Balestra, G. M.; Kenny, J. M.; Torre, L.; Puglia, D. Antioxidant and antibacterial lignin nanoparticles in polyvinyl alcohol/chitosan films for active packaging. *Ind. Crops Prod.* **2016***, 94*, 800-811, DOI 10.1016/j.indcrop.2016.09.061.

31. Nada, A. M. A.; El-Diwany, A. I.; Elshafei, A. M. Infrared and antimicrobial studies on different lignins. *Acta Biotechnol.* **1989***, 9*, 295-298, DOI 10.1002/abio.370090322.